KEK Preprint 95-98
HCMT-9501
KOBE HEP 95-05
KUNS-1358
OUHEP 95-2
OULNS 95-01
TMU-HEP 95-11
September 1995
H

Study of Inclusive Baryon-Antibaryon Pair Production of p or Λ in Two-Photon Processes

VENUS Collaboration

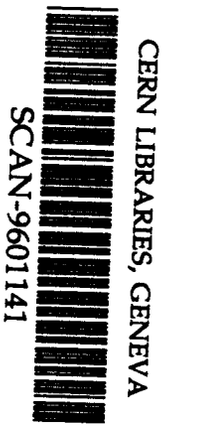

Submitted for Publication.

National Laboratory for High Energy Physics, 1995

KEK Reports are available from:

Technical Information & Library
National Laboratory for High Energy Physics
1-1 Oho, Tsukuba-shi
Ibaraki-ken, 305
JAPAN

Phone: 0298-64-5136
Telex: 3652-534 (Domestic)
(0)3652-534 (International)
Fax: 0298-64-4604
Cable: KEK OHO
E-mail: Library@kekvax.kek.jp (Internet Address)

Study of Inclusive Baryon-Antibaryon Pair Production of p or Λ in Two-Photon Processes

VENUS Collaboration

S.Uehara[1*], K.Abe[2], K.Amako[1], Y.Arai[1], T.Arima[3,a], Y.Asano[3], M.Chiba[4], Y.Chiba[5], M.Daigo[6], M.Fukawa[1], Y.Fukushima[1], J.Haba[7], H.Hamasaki[3], H.Hanai[7], Y.Hemmi[8], M.Higuchi[9], F.Hinode[1], T.Hirose[4], Y.Homma[10], N.Hosoda[4,b] N.Ishihara[1], Y.Iwata[11] J.Kanzaki[1], R.Kikuchi[8], T.Kondo[1], T.T.Korhonen[1,12], H.Kurashige[8], E.K.Matsuda[13], T.Matsui[1], M.Miura[3,c], K.Miyake[8], S.Mori[3], Y.Nagashima[7], Y.Nakagawa[14], T.Nakamura[15], I.Nakano[16], S.Odaka[1], K.Ogawa[1†], T.Ohama[1], T.Ohsugi[11], H.Ohyama[17], K.Okabe[13], A.Okamoto[8], A.Ono[18], T.Oyama[4], J.Pennanen[1,12], H.Sakamoto[8], M.Sakuda[1], M.Sato[9], N.Sato[1], M.Shioden[19], J.Shirai[1], M.Shirakata[3,d], T.Sumiyoshi[1], Y.Takada[3], F.Takasaki[1], M.Takita[7], N.Tamura[13], D.Tatsumi[7], K.Tobimatsu[20], T.Tsuboyama[1], Y.Unno[1], T.Watanabe[21], Y.Watase[1], F.Yabuki[4], Y.Yamada[1], T.Yamagata[14], Y.Yonezawa[22], H.Yoshida[23] and K.Yusa[3]

[1] KEK, National Laboratory for High Energy Physics, Oho 1-1, Tsukuba 305, Japan (Phone:(81)298-64-5342, FAX:(81)298-64-2580)

[2] Department of Physics, Tohoku University, Aza-Aoba, Aramaki, Aoba-ku, Sendai 980, Japan (Phone:(81)22-222-1800 ext.5628, FAX:(81)22-262-0388)

[3] Institute of Applied Physics, University of Tsukuba, Tennoudai 1-1-1, Tsukuba 305, Japan (Phone:(81)298-53-5302, FAX:(81)298-53-5205)

[4] Department of Physics, Tokyo Metropolitan University, Minami-Ohsawa 1-1, Hachioji 192-03, Japan (Phone:(81)426-77-1111 ext.3334, FAX:(81)426-77-2483)

[5] Yasuda Women's Junior College, Yasuhigashi 6-13-1, Asa-Minami-ku, Hiroshima 731-01, Japan (Phone:(81)82-878-8111 ext.237, FAX:(81)82-872-2896)

[6] Faculty of Economics, Toyama University, 3190 Gofuku, Toyama 930, Japan (Phone:(81)764-41-1271 ext.2513, FAX:(81)764-33-8744)

[7] Department of Physics, Osaka University, Machikaneyama 1-1, Toyonaka 560, Japan (Phone:(81)6-844-1151 ext.4130, FAX:(81)6-855-6664)

[8] Department of Physics, Kyoto University, Oiwake-cho, Kita-Shirakawa, Sakyo-ku, Kyoto 606, Japan (Phone:(81)75-753-3852, FAX:(81)75-711-5175)

[9] Department of Applied Physics, Tohoku-Gakuin University, Chuo 1-13-1, Tagajo 985, Japan (Phone:(81)22-368-1115 ext.328, FAX:(81)22-368-7070)

[10] School of Applied Medical Science, Kobe University, Tomogaoka 7-10-2, Suma-ku, Kobe 654-01, Japan (Phone:(81)78-792-2555, FAX:(81)78-793-2713)

[11] Department of Physics, Hiroshima University, Kagamiyama 1-3-1, Higashi-Hiroshima 724, Japan (Phone:(81)824-24-7378, FAX:(81)824-24-0715)

[12] Research Institute for High Energy Physics, Helsinki University, Siltavuorenpenger 20C SF-00170, Helsinki, Finland

[13] Department of Physics, Okayama University, Tsushimanaka 3-1-1, Okayama 700, Japan (Phone:(81)86-251-7817, FAX:(81)86-252-7595)

[14] Division of Natural Sciences, International Christian University, Ohsawa 3-10-2, Mitaka 181 Japan (Phone:(81)422-33-3263, FAX:(81)422-33-1449)

[15] Faculty of Engineering, Miyazaki University, Gakuen-Kibanadai-Nishi 1-1, Miyazaki 889-01,

Japan (Phone:(81)985-58-2885, FAX:(81)985-58-2876)
[16] Institute of Physics, University of Tsukuba, Tennoudai 1-1-1, Tsukuba 305, Japan (Phone:(81)298-53-4253, FAX:(81)298-53-4491)
[17] Hiroshima National College of Maritime Technology, Higashino-cho 4272-1, Hiroshima-ken 725-02, Japan (Phone:(81)8466-5-3101, FAX:(81)8466-5-2947)
[18] Faculty of Cross-Cultural Studies, Kobe University, Tsurukabuto 1-2-1, Nada-ku, Kobe 657, Japan (Phone:(81)78-803-0741, FAX:(81)78-803-0833)
[19] Department of Electronic and Computer Engineering, Ibaraki College of Technology, Nakane, Hitachinaka 312, Japan (Phone:(81)29-271-2955, FAX:(81)29-271-2813)
[20] Center for Information Science, Kogakuin University, Nishi-Shinjuku 1-24-2, Shinjuku-ku, Tokyo 163-91, Japan (Phone:(81)3-3340-0134, FAX:(81)3-3340-0135)
[21] Department of Physics, Kogakuin University, Nakano-cho 2665-1, Hachioji, Tokyo 192, Japan (Phone:(81)426-22-9291 ext.3258, FAX:(81)426-27-4587)
[22] Tsukuba College of Technology, Kasuga 4-1, Tsukuba 305, Japan (Phone:(81)298-58-9576, FAX:(81)298-58-9579)
[23] Naruto University of Education, Naruto-cho, Naruto 772, Japan (Phone:(81)886-87-1311, FAX:(81)886-87-1090)

* Internet address: uehara@kekvax.kek.jp
† Deceased
[a] Present address: Department of Nuclear Engineering, Kyushu University, Hakozaki, Fukuoka 812, Japan
[b] Present address: Japan Synchrotron Radiation Research Institute, Kanaji 1503-1, Kamigouri-cho, Hyogo-ken 678-12, Japan
[c] Present address: Institute for Cosmic Ray Research, University of Tokyo, Tanashi 188, Japan
[d] Present address: KEK, National Laboratory for High Energy Physics, Oho 1-1, Tsukuba 305, Japan

Abstract

Baryon-antibaryon pair production was studied in two-photon events which were collected at the e^+e^- collider TRISTAN, and correspond to an integrated luminosity of 303 pb^{-1}. Correlations between a baryon and an antibaryon were studied for their flavors (p or Λ) and their momentum vectors. The experimental results were compared with the expectations from a jet-fragmentation Monte Carlo simulation. We have found that although the ratios of the cross sections of different baryon-flavor combinations are consistent with the Monte Carlo expectations, the cross section shows an excess over the Monte Carlo expectation at a low invariant-mass region of final-state particles at large angles. The experimental data show no narrow azimuthal-angle correlation, which is expected from a jet-fragmentation Monte Carlo. A search for exclusive Λ pair production has also been made. We have no candidates and have obtained the upper limit for the cross section.

1 Introduction

The Λ baryon carries two quantum numbers: the strangeness and the baryon number. Studies of their production in two-photon processes provide valuable information concerning s-quark production, the baryonization mechanism and correlations between them. Two-photon processes at high energies have a large variety of subprocesses in hadronic production. In the direct process (QPM), in which the two photons couple with a quark line by QED couplings[1], the s-quark production is greatly suppressed compared with that of the u-quark because the cross section is proportional to the fourth order of the electric charge. However, s-production from a gluon(s) in resolved photon processes[2] and production in a stage of hadronization are not very suppressed because the QCD coupling is universal for quark flavors. Therefore, the production rate of strange particles is sensitive to the production mechanism in two-photon processes.

Baryon production from two-photon collisions shows an excess over the QCD prediction in exclusive $p\bar{p}$ production, $\gamma\gamma \to p\bar{p}$, which has been extensively studied[3, 4, 5]. The excess is considered to come from a long-distance or diquark effect[6]. However, the cross section quickly dumps with the c.m. energy of the two-photon system, and is difficult to measure above 3.0 GeV, where the capability in the QCD prediction is expected to increase. It could be very interesting to search for the excess at higher energies in inclusive baryon-antibaryon ($\mathcal{B}\bar{\mathcal{B}}$) production. Baryonization is considered to be well explained within the framework of the string jet-fragmentation model at a much higher energy region in the e^+e^- annihilation process[7, 8]. We will be able to obtain information concerning baryonization at "intermediate" energies by two-photon collisions using a high-energy e^+e^- collider. The correlations of a baryon and an antibaryon in the same event for baryon flavors ($\mathcal{B}\bar{\mathcal{B}}$ combinations as $p\bar{p}$, $\Lambda\bar{p}$, $p\bar{\Lambda}$ or $\Lambda\bar{\Lambda}$) and for momentum vectors give valuable information concerning the production mechanism of baryon pairs and s-quarks.

The TOPAZ collaboration has reported on the result of their Λ-inclusive production measurement in two-photon processes[9]. They found an excess of Λ production over the expectation based on a calculation which included the resolved photon processes which reproduce their K_S-inclusive production data[10]. They explained that this excess came from a higher-order QCD effect. We can study the excess in relation to the $\mathcal{B}\bar{\mathcal{B}}$ correlations, not only for Λ-inclusive events, but also for $p\bar{p}$-inclusive events.

We have measured the inclusive $\mathcal{B}\bar{\mathcal{B}}$ production. The Λ was identified by a reconstruction of $\Lambda \to p\pi^-$. Although the requirement of a baryon and an antibaryon in an event reduces the event statistics, it enables us to study the correlations of a baryon and an antibaryon. In the case that the production cross section, itself, is not well explained by the known models, it is essentially necessary to measure the various kinematical information in order to understand the detailed production mechanism.

The exclusive Λ pair production $\gamma\gamma \to \Lambda\bar{\Lambda}$, which has not yet been observed experimentally[11], has also been searched using a similar analysis procedure as that for the inclusive processes.

2 VENUS Detector

The data were collected using the VENUS detector at the TRISTAN e^+e^- collider at KEK. An overview of the VENUS detector has been given elsewhere[12]. Here, we explain the detector components used in this analysis.

The central drift chamber (CDC)[13] detects charged tracks in a polar angle region of $|\cos\theta| \leq 0.85$ with a momentum resolution of $\sigma_p/p = \sqrt{(0.013)^2 + (0.008 p_T[\mathrm{GeV}/c])^2}$ for tracks with sufficient number of hits, where p_T is the transverse momentum of the track with respect to the beam axis. The polar and azimuthal angle resolutions for energetic particles, whose Coulomb and nuclear scattering can be neglected, are $\sigma_\theta = 8\sin^2\theta$ mrad and $\sigma_\varphi = 1$ mrad, respectively. Protons and antiprotons were identified with time-of-flight counters (TOF)[14] whose time resolution was 250 ps at $|\cos\theta| \leq 0.80$. The distance from the collision point to the counters was 166 cm in the $\theta = 90°$ direction. The CDC and TOF were installed in a superconducting solenoid which provided a uniform field of 0.75 T parallel to the beam direction.

Two types of electromagnetic calorimeters, the lead glass calorimeter (LG) [15] and the liquid argon calorimeter (LA)[16], measured the energy deposit of the particles in the polar angle regions $|\cos\theta| \leq 0.80$ and $0.79 \leq |\cos\theta| \leq 0.99$, respectively, with the energy resolutions of $\sigma_E/E = (2.5 + 7.0/\sqrt{E})\%$ and $(1.6 + 10.0/\sqrt{E})\%$, respectively.

3 Data Collection

The data were taken at c.m. energies ranging from 57 to 62 GeV, with the an average c.m. energy ($<\sqrt{s}>$) of 58.0 GeV. The total integrated luminosity was 303 pb^{-1}. The VENUS detector was upgraded during the data-collection period by adding a transition radiation detector and replacing the inner chamber with a vertex chamber and a trigger chamber. In this upgrade, the beam pipe and beam masks were also replaced. Eighty percent of the data were collected after the upgrade. In the present analysis, the data quality was not much changed by the upgrade, because we did not use the newly installed or replaced detector components. The change in the material quantity due to the upgrade was taken into account at the correction stage; its systematic effect was smaller than the systematic errors caused by other sources.

The data sample for the present analysis was taken by three types of event triggers. The LG total energy sum trigger ($\mathrm{LG_{tot}}$) required a total energy deposit in the LG larger than 3 GeV. The trigger " $\mathrm{LG_{seg}} * \mathrm{TF} \geq 2$ " required an energy deposit larger than 0.6 GeV in at least one LG segment (the LG was divided into 58 segments) and two or more CDC tracks with $p_T \geq 0.6$ GeV/c and $|\cos\theta| \leq 0.89$ were identified by the fast track-finding electronics (TF). A track trigger required two or more CDC tracks to hit near to the TOF counters. In the trigger, an acoplanarity angle of at least one arbitrary track pair with a transverse momentum of each track larger than 0.6 GeV/c must be less than 25° in the majority of the runs, where the acoplanarity angle is defined by the supplement of the opening angle of the two tracks projected onto the plane perpendicular to the beam axis

($r\varphi$ plane). We did not use the events triggered only by the LA energy deposit in order to define a definite acceptance for events in which the particles were observed at large angles.

4 Event Selection

In this paper we discuss our analysis of $\mathcal{B}\bar{\mathcal{B}}$-inclusive events ($\mathcal{B}$ indicates p or Λ) and $\Lambda\bar{\Lambda}$-exclusive events from two-photon collisions. We selected those events which included a proton and an antiproton based on the following criteria: 1) The total visible energy measured by the CDC, the LG and the LA be smaller than 15 GeV. 2) A proton and an antiproton candidate with $|\cos\theta| \leq 0.80$, $0.45 \leq p_T \leq 1.5$ GeV/c, $|r_{\rm min}| \leq 2$ cm and $|z_{\rm min}| \leq 10$ cm be found, where $|r_{\rm min}|$ is the distance of the track to the beam axis at the closest approach, and $|z_{\rm min}|$ is the distance of the point which gives $|r_{\rm min}|$ to the collision point along the beam direction. 3) At least one other charged track with $|\cos\theta| \leq 0.85$, $p_T \geq 0.1$ GeV/c, $|r_{\rm min}| \leq 5$ cm and $|z_{\rm min}| \leq 15$ cm existed. Criterion 1) rejected the e^+e^- annihilation events, and almost all single-tagged events in which a recoil electron hit the LA. In 2), the protons and antiprotons were selected by a TOF cut corresponding to $\leq 5\sigma$, where σ is the resolution which arises from the accuracies of the TOF and momentum measurements, and by applying an additional cut for the reconstructed mass, $m_{\rm TOF} \geq 0.75$ GeV/c^2, in order to reduce the background from the $\pi^\pm$ and $K^\pm$ in the high-momentum region. Figure 1 shows the $m_{\rm TOF}$ distributions for charged particles with $0.45 \leq p_T \leq 1.5$ GeV/c in events including a proton or an antiproton candidate and satisfying criteria 1) and 3). The excess of negatively charged particles over positively charged particles comes from the protons produced by the scatterings of beam particles on residual gas nuclei or the beam pipe. Most of these events were rejected by requiring both a proton and an antiproton (see subsection 6.6). Criterion 3) was set to reject events containing only $p\bar{p}$ candidates as visible tracks. The $|r_{\rm min}|$ and $|z_{\rm min}|$ cuts in 2) and 3) were made sufficiently loose in order to detect $\Lambda \to p\pi^-$ decays with high efficiency. After event selections, 1557 events remained.

5 Λ Reconstruction

The Λ (the names of particles in this subsection include the corresponding antiparticles) were reconstructed in the following way. A proton candidate was combined with the oppositely-charged track which passed through the criteria written in 3) in the previous section. The crossing point of the two tracks in the $r\varphi$ plane was assumed to be a decay point. Even in the case that the both tracks did not cross with a closest distance of less than 0.5 cm in the $r\varphi$ plane, the decay point was assumed to be the medium point of the distance. The decay length (ℓ) was defined as the distance between the decay point and the collision point in the $r\varphi$ plane. A minus sign was given for ℓ when the azimuthal angle difference between the vector connecting the collision point with the decay point and the combined momentum vector of the decay products was larger than 90°. Because there

are two crossing points in the usual case, we selected that which had a smaller absolute value of ℓ, except for the case that $\ell \leq -2$ cm, for which we selected the positive ℓ, if it existed. The Λ candidates were required to satisfy the criteria $|m_{p\pi} - M_\Lambda| \leq 15$ MeV/c^2 and $+1.5 \leq \ell \leq 30$ cm, where $m_{p\pi}$ is the invariant mass of the two tracks calculated by using the proton and charged-pion masses. Figure 2 shows the invariant-mass distributions before and after the decay-length cut. The resolution of the invariant mass was about 3.8 MeV/c^2 at the core of the peak. The slope in the decay length distribution was in good agreement with that expected from the lifetime of Λ. The momentum vector of the Λ candidate was defined as the summed momentum at the decay point. Extra cuts, $|\cos\theta| \leq 0.80$ and $0.45 \leq p_T \leq 1.5$ GeV/c, were applied for the momentum of the Λ candidates.

6 Baryon-Antibaryon Inclusive Processes

6.1 Event classification

The selected events were categorized into three groups: $p\bar{p}X$ events, $\Lambda\bar{p}X$ or $p\bar{\Lambda}X$ events and $\Lambda\bar{\Lambda}X$ events, where Λ ($\bar{\Lambda}$) was for candidates reconstructed by the method written in the previous section, and p ($\bar{p}$) the proton (the antiproton) candidates which were not reconstructed to Λ ($\bar{\Lambda}$). The events with no extra charged track (X) which satisfied the criterion for tracks written in 3) in section 4 with a more severe $|r_{\rm min}|$ cut, $|r_{\rm min}| \leq 2$ cm (we call this criteria the " selection criteria for X"), were rejected in order to select only "visibly inclusive" events. The 2.7% fraction of the selected events which contained two or more same-sign baryons were also rejected. Finally, we required the transverse momenta of both $\mathcal{B}$ and $\bar{\mathcal{B}}$ be larger than 0.6 GeV/c and less than 1.5 GeV/c in order to ensure sufficient trigger and detection efficiencies and to reduce the background contamination. We corrected p_T of the baryons for energy losses in the detector material before the cut. The numbers of $p\bar{p}X$, $\Lambda\bar{p}X$, $p\bar{\Lambda}X$, and $\Lambda\bar{\Lambda}X$ events were 824, 52, 55 and 7, respectively.

The invariant mass of the incident two-photon system (W) is one of the most important kinematical parameter of the events. However, we cannot measure it, due to the limited angular coverage of the detector. In the resolved photon process, a non-negligible fraction of the hadronic energy flows to forward angles where a precise momentum and/or energy measurement is very difficult. We therefore, defined the invariant mass of the central part ($W_{\rm C}$) as consisting of the final-state particles with $p_T \geq 0.1$ GeV/c emitted in the polar angle region $|\cos\theta| \leq 0.85$. $W_{\rm C}$ is a measure of the c.m. energy of the hard-scattering part, not only in the direct process, but also in the resolved photon processes. We defined $W_{\rm Cvis}$ as a visible invariant mass combined for observed particles in $|\cos\theta| \leq 0.85$ by assigning the respective mass values to $\Lambda(\bar{\Lambda})$, $p(\bar{p})$ and $K^\pm$ candidates[1], and assigning the pion mass to other charged tracks satisfying the selection criteria for X. The electromagnetic clusters in the LG and LA of $E \geq 0.2$ GeV, being not connected with any charged

[1]The charged kaons were selected with $\leq 2\sigma$ TOF cut in the charged particles which are not identified as p or $\bar{p}$ and whose $p_T \leq 0.9$GeV/c.

track, were also included in $W_{\rm Cvis}$, except for LG clusters near to the extrapolated $\bar{p}$ track within 25° of the opening angle, so as not to doubly count the associated energy of $\bar{p}$ annihilation in the detector material. We show in Fig.3 the obtained $W_{\rm Cvis}$ distributions of the three groups of the $\mathcal{B}\bar{\mathcal{B}}$-inclusive events within the range $2 < W_{\rm Cvis} < 9$ GeV/c^2.

6.2 Monte Carlo calculations

We carried out Monte Calro (MC) calculations in order to study s-quark or Λ production, as follows. Those events from a direct process were generated by the code of Berends et al.[17] for $u\bar{u}$, $s\bar{s}$ and $c\bar{c}$ production. The LUND fragmentation model in JETSET7.3 (for Matrix Element)[18] with default parameters was used for hadronization. The contribution from the $d\bar{d}$ in the direct process was $\sim 1/16$ of $u\bar{u}$, and was safely neglected for the present accuracy of the calculation. We also neglected the contribution of the VDM process. According to the low-p_T subprocesses in PYTHIA5.7 connected with JETSET7.4(for Parton Shower)[19], and taking the known total hadronic cross section of the two-photon processes into account[20], the production rate of baryons with $p_T \geq 0.6$ GeV/c was negligibly small due to a steep decrease in the cross section with p_T.

The resolved photon processes were calculated by PYTHIA5.7 with JETSET7.4 for diagrams including u-, d-, s- and c-quarks and gluons. The default parameters of PYTHIA5.7 and JETSET7.4 were used, except for the parton density functions in a photon and the $p_T^{\rm min}$ value. For primary $c\bar{c}$ production, we used the parton densities from LAC1 parametrization[21], which shows a reasonable agreement with the experimental data for open charm production[22, 23]. We used DG parametrization[24] for primary production of lighter quarks and gluons because LAC1 requires a high momentum-cut value for $p_T^{\rm min}$ at around 2.2 GeV/c to reproduce the jet spectra[25]. Such a high $p_T^{\rm min}$ value can make an unphysical bias for an event sample with low-$W_{\rm C}$ (less than 4 GeV/c^2) and only low-p_T (less than 1 GeV/c) particles. The DG parametrization well reproduces the jet spectra data with a relatively low $p_T^{\rm min}$ value[25]. We set the $p_T^{\rm min}$ value at 1.4 GeV/c, which is slightly lower than the best value to reproduce the experimental jet spectra, because the VDM-like contribution might still exist to fill the gap between a hard component, described by resolved photon processes, and a soft component by the VDM processes. Using the different parametrization for charm production from that for light-quark or gluon production is allowed at the present stage because charm production is dominated by only the gluon component in a photon with a limited x range, which is not well determined by measurements of the jet spectra.

We generated MC events with the amount corresponding to an integrated luminosity of about three-times the experimental value. The MC events were divided into the following four classes according to the types of s-quark or Λ production:

1) direct processes of $u\bar{u}$ and $c\bar{c}$ production,

2) resolved photon processes other than the primary $s\bar{s}$ production,

3) primary $s\bar{s}$ production in direct and resolved photon processes,

4) Λ ($\bar{\Lambda}$) production as a decay product of Λ_c ($\bar{\Lambda}_c$) in primary $c\bar{c}$ production in the direct and resolved photon processes.

In 1), the contribution from $d\bar{d}$ was safely neglected (as mentioned above). The contribution from the resolved photon process is much larger than that from the direct process in 3).

Detector and trigger simulations were applied for the MC events. The events were passed through the same selection criteria as those applied for the real events. Corrections to the detector efficiencies were made of effects which were not taken into account in the detector simulator (the details are mentioned in subsection 6.6). The predictions of the MC calculations are shown in Fig.3 by histograms.

6.3 Topological cross section for $p\bar{p}$-inclusive events

The Λ reconstruction efficiency in our analysis is estimated to be less than 50% for the entire p_T region, because the momentum of the charged pion from the decay is so small that a part of them is rejected by a p_T cut of 0.10 GeV/c. This means that there are many unreconstructed Λ's which are identified as sole protons. We can obtain the production cross sections for the $p\bar{p}X$, $\Lambda\bar{p}X$ or $p\bar{\Lambda}X$ and $\Lambda\bar{\Lambda}X$ processes separately using the estimated inefficiency. However, such a procedure produces an additional error correlated among the processes. Furthermore, it is difficult to obtain the differential cross sections ($d\sigma/dW_{\rm C}$) for individual process because of a limited event statistics. We present the "summed" cross section of these processes, i.e. "topological cross section for $p\bar{p}$-inclusive events" regardless of the origins of p and $\bar{p}$ in this subsection, and present the ratios among them in the next subsection.

We have obtained the topological cross section for $p\bar{p}$-inclusive events in anti-tagged two-photon processes, which corresponds to:

$$\begin{aligned}\frac{d}{dW_{\rm C}}\{ \quad & \sigma[e^+e^- \to e^+e^-p\bar{p}X] \\ + \ & (\sigma[e^+e^- \to e^+e^-\Lambda\bar{p}X] + \sigma[e^+e^- \to e^+e^-p\bar{\Lambda}X])B(\Lambda \to p\pi^-) \\ + \ & \sigma[e^+e^- \to e^+e^-\Lambda\bar{\Lambda}X](B(\Lambda \to p\pi^-))^2 \ \} \end{aligned} \tag{1}$$

for kinematical conditions:

$$\begin{aligned}\sqrt{s} = 58 \text{ GeV}, \ |\cos\theta(\mathcal{B},\bar{\mathcal{B}})| \le 0.80, \ 0.6 \le p_T(\mathcal{B},\bar{\mathcal{B}}) \le 1.5 \text{ GeV}/c, \\ X \ge 1 \text{ prong}, \ |\cos\theta(X)| \le 0.85, \ p_T(X) \ge 0.1 \text{ GeV}/c,\end{aligned} \tag{2}$$

where $B(\Lambda \to p\pi^-)(= 0.64)$ is the branching ratio. The unfolding method was used to obtain the topological cross section from the measured numbers of $\mathcal{B}\bar{\mathcal{B}}X$ events. We fit

the cross-section values at W_C from 2.5 to 10.5 GeV/c^2 with 1.0 GeV/c^2 steps to the experimental W_{Cvis} distribution summed over the three groups of the $\mathcal{B}\bar{\mathcal{B}}X$ events using a correction matrix, where an element of the correction matrix (w_{ij}) was defined as the probability that an event in the j-th W_C bin survives the selection, and is found in the i-th W_{Cvis} bin. In order to obtain a solution with a smooth W_C dependence, we used an assumed W_C dependence of the topological cross section, $\sim (W_C - 2.2[\mathrm{GeV}/c^2])^a W_C^{-b}$ (both a and b should be positive numbers), as a loose constraint by adding an extra contribution to χ^2, $\Delta\chi^2 = [(d\sigma/dW_C) - (d\sigma/dW_C)_{curve}]^2/[0.5(d\sigma/dW_C)]^2$, at each W_C point, where $(d\sigma/dW_C)$ and $(d\sigma/dW_C)_{curve}$ are a fitting result and the value on the curve of the assumed W_C dependence, respectively. We used two kinds of the correction matrices to check the systematic error caused by the choice of the correction matrix. One was made by the MC events from $u\bar{u}$ production in the direct process; the other was made by those from the resolved photon processes except for the primary $s\bar{s}$ production. In the matrices, the relation between W_C and W_{Cvis} showed a good linearity, $W_{Cvis} \approx 0.90 W_C$, for the direct process, and $\approx 0.85 W_C$ for the resolved photon processes. A small difference in the factors comes from a difference in an event shape in the two processes; the events from the resolved photon processes have more activities at the forward angles than those from the direct process. However, the results from the two correction matrices coincided well, except for the ones at the lowest W_C bin, where we treated the difference as a systematic error.

Figure 4 shows the topological cross section defined by Eqs.(1) and (2). We do not present the results at $W_C > 9$ GeV/c^2, because the systematic error from the unfolding is large there. The curves are a prediction of the MC calculations for the direct processes and the sum of the direct and the resolved photon processes. The experimental data show an excess over the prediction at $W_C \leq 5$ GeV/c^2. Above 6 GeV/c^2, the data seem to be slightly smaller than the prediction.

6.4 Baryon-antibaryon flavor ratios

The ratios among the cross sections of different baryon-antibaryon flavor combinations ($\mathcal{B}\bar{\mathcal{B}}$ flavor ratios) were obtained after the correction, taking the p_T-dependent Λ reconstruction efficiency estimated by the detector simulator into account. The combinatorial background in Λ samples was also corrected. The same kinematical conditions as applied to the topological cross section, (2) in the previous subsection, within a W_C range of $2 \leq W_C \leq 9$ GeV/c^2, were used. The branching ratio ($B(\Lambda \to p\pi^-)$) was used to obtain the ratios for Λ's, including all of the decay modes. Based on the definition given here, "p" includes protons from the decay of any hadrons, except for Λ: protons from $\Delta \to p\pi$, $\Sigma^+ \to p\pi^0$ and so on. However, "Λ" includes all decay products, such as Λ's from $\Sigma^0 \to \Lambda\gamma$, $\Lambda_c \to \Lambda$ + something and so on. The results are

$$(\sigma[p\bar{\Lambda}X] + \sigma[\Lambda\bar{p}X])/\sigma[p\bar{p}X] = 0.58 \pm 0.09 \pm 0.06$$
$$\sigma[\Lambda\bar{\Lambda}X]/\sigma[p\bar{p}X] = 0.10 \pm 0.06 \pm 0.02.$$

The first errors are statistical and the second systematic (see the subsection 6.6). The boundary effect for a limited $W_{\rm Cvis}$ range was studied based on the MC events. We found that the effect was negligibly small compared to other systematic errors. We therefore did not make any unfolding for the flavor ratios. Figure 5 compares the result with the MC expectations from s-quark or Λ production in hadronization in direct and resolved photon processes, and from the total contribution. The experimental results are consistent with the MC expectations.

6.5 Correlations in the azimuthal angles and rapidities

Another important correlation of the $\mathcal{B}\bar{\mathcal{B}}$ is that of their momentum vectors. In two-photon processes, where the energies of the incident photons are not known, the p_z component of an emitted particle is not a direct quantity of the scattering. We use the opening angles in the $r\varphi$ plane ($\Delta\varphi$) and the rapidity difference (Δy) as observables. It is noted that they are invariant for Lorentz boosts along the beam direction. At the low-$W_{\rm C}$ region, in which the masses for $\mathcal{B}$ and $\bar{\mathcal{B}}$ are not negligible compared with $W_{\rm C}$, $\Delta\varphi$ has a tendency to strongly concentrate around 180° to balance p_T. To examine the dynamical effect not restricted by the kinematics, we used events with $W_{\rm Cvis} \geq 5$ GeV/c^2 only in this subsection.

Figures 6(a), (b) and (c) show the data for the $\Delta\varphi$ distributions compared with the MC results for $p\bar{p}X$, $p\bar{\Lambda}X$ or $\Lambda\bar{p}X$ and $\Lambda\bar{\Lambda}X$ events, respectively. There are peaks around 0° and 180° in the MC results. However, no peaks were found around 0° in the experimental data for $p\bar{p}X$ and $p\bar{\Lambda}X$ or $\Lambda\bar{p}X$ events, and they are rather flat. We checked whether the selected events had something like a jet structure by watching the $\Delta\varphi$ distributions between a baryon (an antibaryon) and other charged tracks than an antibaryon (a baryon) candidate with $0.6 \leq p_T \leq 1.5$ GeV/c and $|\cos\theta| \leq 0.80$ (Fig. 6(d)). No prominent 0° peak, i.e. no strong jet structure, was found in either experimental data and the MC. Around 180°, the experimental data are consistent with the MC in all of the $\Delta\varphi$ distributions.

Figure 7 shows similar distributions for the rapidity difference (Δy). Generally, the number of pairs increases toward small Δy. This partly comes from the detection efficiency due to the limited polar angle coverage of the detector. However, the behaviors of Δy near to 0 have significant meanings, because the efficiency dependence is small there. The experimental data seem to be consistent with the prediction of MC.

6.6 Corrections, backgrounds and systematic errors

We now summarize the corrections applied in the present analysis, background estimation and systematic errors. The corrections described in this subsection have already been applied to the presented topological cross section and the $\mathcal{B}\bar{\mathcal{B}}$ flavor ratios. However, the presented numbers of events for the experimental data are always those actually observed,

and they included background. The MC expectations are presented after a correction of the efficiencies, and do not include the background.

Corrections and backgrounds: A minor modification of the trigger conditions, the response of the calorimeters for hadrons and nuclear interactions in the detector material were not fully taken into account in the detector simulator, even though they affected the trigger and detection efficiencies. We corrected the effect for the MC expected number of events, the topological cross section and the $\mathcal{B}\bar{\mathcal{B}}$ flavor ratios. The correction factor was typically 20% in each of the present results.

The contamination of $\pi^{\pm}$ or $K^{\pm}$ in p ($\bar{p}$) candidates must be corrected, when obtaining the topological cross section. We estimated the contamination in p ($\bar{p}$) samples by investigating $\bar{p}$-inclusive (p-inclusive) events in the experimental data. We found that the misidentification probability of $\pi^{\pm}$ or $K^{\pm}$ as p ($\bar{p}$) was $0.7 \pm 0.2\%$ of the $\pi^{\pm}$ and $K^{\pm}$ samples. Consequently, the background fractions were estimated to be 2% for p candidates and 6% for $\bar{p}$ candidates. The 4% excess in $\bar{p}$ came from p-inclusive beam background events due to beam collisions with residual gas or the beam pipe, where p's are actually produced, and $\bar{p}$'s are from particle misidentification. The quantity of the excess is consistent with that estimated from the $z_{\rm min}$ distribution of candidate p and $\bar{p}$.

The measurement of the $\mathcal{B}\bar{\mathcal{B}}$ flavor ratios is sensitive to the combinatorial background in the Λ reconstruction. We corrected the ratios for the background, which was about 1.3% of the protons and about 20% of Λ candidates. The difference of the $\pi^{\pm}$ or $K^{\pm}$ contamination ratios in p ($\bar{p}$) samples must also be corrected; the Λ sample has been passed through the severe cut criteria in the Λ reconstruction and is expected to have higher purity for protons of the decay products than in a "originally produced" proton sample.

The p and Λ can be produced by scatterings of $\pi^{\pm}$ and K^{-} or $\bar{K}^{0}$, respectively, on the detector materials. Such backgrounds were estimated to be small, $\sim 2\%$ of the p candidates and less than 1% of the Λ sample, respectively, because the purity of baryons was increased by tagging an antibaryon in the same event. Other background, such that the whole event was from the interaction on beam pipe or residual gas nucleus in spite of the fact that both the p and $\bar{p}$ were correctly identified, was negligibly small. The background from the $e^{+}e^{-}$ annihilation process was estimated to be less than 1% by MC and can be safely neglected.

Systematic errors: Systematic errors caused by ambiguities of the above-mentioned corrections are 4% due to the changes in the trigger conditions, 7% from nuclear scattering, and 3% from a background estimation for particle misidentification. The other source is from the detector response. The ambiguity of the TOF resolution causes a 5% systematic error. A possible systematic shift of the energy scale in calorimetry causes an error of 3% at $W_{\rm Cvis} \leq 9$ GeV/c^2 in the $E_{\rm vis}$ cut. A further systematic error in the topological cross section comes from the unfolding. It was estimated by using different MC samples for the direct process and for the resolved photon processes. The $\mathcal{B}\bar{\mathcal{B}}$ flavor ratios have another source of the systematic error, coming from the estimated Λ reconstruction efficiency. We have estimated the systematic error for the efficiency to be 5%.

Consequently, the systematic error for the topological cross section is around 12%,

except for 32% at the lowest $W_{\rm C}$ bin, where we added the systematic errors in quadrature. The MC expected number of events include a systematic error of 9% for $p\bar{p}$-, 10% for $\Lambda\bar{p}$- or $p\bar{\Lambda}$- and 13% for $\Lambda\bar{\Lambda}$-inclusive data, respectively. Furthermore, predicted cross sections and number of events have ambiguities around 20% based on theoretical calculations, the choices of the QCD energy scale and p_T distribution of the partons in a photon. The systematic errors for the $\mathcal{B}\bar{\mathcal{B}}$ flavor ratios are presented in subsection 6.4.

6.7 Discussion on $\mathcal{B}\bar{\mathcal{B}}$-inclusive processes

The observed topological cross section shows a deficit of the MC expectation at $W_{\rm C} < 5$ GeV/c^2. This tendency is seen in both the $p\bar{p}X$ and $\Lambda\bar{p}X$ ($p\bar{\Lambda}X$) events, as shown in Fig.3, and the $\mathcal{B}\bar{\mathcal{B}}$ flavor ratios are consistent with the MC expectations. Therefore, the deficit is considered to result from some defect in baryonization in the models at the low-$W_{\rm C}$ region, and not from the production ratio of s-quarks to u- and d-quarks in the hadronization stage. Possible sources of the deficit are neglecting VDM (or very small expectation from a VDM model we used is wrong), the parameters in the calculation, such as the parton densities or the $p_T^{\rm min}$, and validity of the calculations based on the perturbative-QCD among point-like partons.

The first two possibilities are deeply connected with each other. We can say that the VDM process is a phenomenological component of a hadronic interaction of a photon to describe its soft part. The p_T dependence is usually expressed by an exponential-type function to describe only low-p_T nature of the interaction. According to the present idea concerning the VDM, it is impossible to add the high-p_T component, because it must be accounted for as an effect from the resolved photon processes, which bear the hard part of the hadronic interactions. A calculation of the resolved photon process has a large problem concerning the $p_T^{\rm min}$ parameter. Usually, $p_T^{\rm min}$ is set much higher than 1.0 GeV/c to fit the experimental jet data. Therefore, the calculation does is not reliable at the p_T region, around or lower than $p_T = p_T^{\rm min}$. However, in the VDM calculation, the cross section is already dumped at around $p_T = p_T^{\rm min}$, and there is a gap between VDM and the resolved photon calculation. Although this gap effect is not serious for the high-p_T jet spectra, it may be important in the low-p_T region for low-$W_{\rm C}$ events where the baryon mass cannot be neglected. It is necessary to improve the model calculations in the low-p_T region around $p_T^{\rm min}$.

The last possibility is related to the primary diquark production. We have no diagram in which the diquark primarily couples with photon(s) or gluon(s) in the MC models. Excess in exclusive $p\bar{p}$ production over the QCD expectation at around $W \approx 3$ GeV/c^2 might also come from primary diquark production[3, 4, 6]. The Λ-inclusive process measured by TOPAZ shows such an excess, for which they gave an explanation that this is due to the QCD higher-order effect[9]. Our data indicate that the $\mathcal{B}\bar{\mathcal{B}}$ flavor ratios are well explained by the s-quark ratios in the jet-fragmentation stage in the MC, and that a higher-order QCD effect exists in the baryonization mechanism in the low-$W_{\rm C}$ region.

We examined the p_T distributions of baryons in order to determine whether the deficit appears in some limited p_T region (Fig.8). However, the shape predicted by the

MC is consistent with the experimental data. Furthermore, no significant shape difference has been found among the MC predictions for subprocesses.

At $W_{\rm Cvis} > 5$ GeV/c^2, the topological cross section and the $\mathcal{B}\bar{\mathcal{B}}$ flavor ratios are consistent with the MC expectations. This indicates that the Λ production in two-photon processes is dominated by production from the "sea" during the hadronization stage. The $\Delta\varphi$ distributions for $p\bar{p}X$ and $\Lambda\bar{p}X$ ($p\bar{\Lambda}X$) at this $W_{\rm Cvis}$ region are different from those of the MC expectations. The MC expectations have peaks at around 0°, while the data show rather flat distributions at $\Delta\varphi < 140°$. However, $\Delta\varphi$ between a baryon and the particles other than an antibaryon (Fig.6(d)) of the MC prediction does not show such a feature. This indicates that while the MC expects production of narrow-angle baryon pairs at the last stage of jet fragmentation, the experimental data show that it is less prominent.

The behaviors at around 180° in the $\Delta\varphi$ distributions and the rapidity difference (Δy) distributions are consistent between in the data and the MC. They show no excess of $\mathcal{B}\bar{\mathcal{B}}$ pairs with a back-to-back topology. The effect of the primary diquark-pair production, which is not taken into account in the MC, is not seen, at least in the high-$W_{\rm C}$ region. Furthermore, since the gross features of $\Delta\varphi$ and Δy are consistent between the MC and the data for all $\mathcal{B}\bar{\mathcal{B}}$ combinations, we can say that the MC well reproduces the Λ-production and/or s-quark production at $W_{\rm C} > 5$ GeV/c^2.

7 Search for $\gamma\gamma \to \Lambda\bar{\Lambda}$ Events

In the exclusive $\mathcal{B}\bar{\mathcal{B}}$ production from two-photon collisions, $\gamma\gamma \to p\bar{p}$ has been measured in several experiments[3]. However, for the hyperon pair production processes, definite cross section values are not yet known. A crude upper limit for $\Lambda\bar{\Lambda}$ production and a rough estimation of the summed cross section of neutral-hyperon pairs are only reported[11].

7.1 Data reduction

We searched for exclusive events, $\gamma\gamma \to \Lambda\bar{\Lambda}$, in the present event sample. We set additional selection criteria to those mentioned in section 4: there were Λ and $\bar{\Lambda}$ candidates satisfying the condition in section 5; also there was no extra tracks reconstructed, and no neutral electromagnetic clusters, $E \geq 0.2$ GeV, in the LG and the LA with an opening angle larger than 25° relative to the antiproton. No candidate remained after the selection. The acceptance of the whole selection was calculated by the MC using the equivalent photon approximation at $2.6 \leq W \leq 3.6$ GeV/c^2, assuming a flat angular distribution at the angle range, $|\cos\theta^*| \leq 0.6$, where θ^* is a scattering angle of Λ in the c.m. frame of the two-photon system, and W the c.m. energy of the two-photon system. The systematic error is estimated to be 15%, which mainly comes from the ambiguity of the Λ reconstruction efficiency. This error is taken into account by raising the upper limit with the same ratio to have a conservative result.

7.2 Results and discussion on $\Lambda\bar{\Lambda}$-exclusive production

We have obtained two kinds of upper limits at the 95% confidence level of the cross section for $|\cos\theta^*| \leq 0.6$ in the W range between 2.6 and 3.6 GeV/c^2 (Fig.9). One is obtained by assuming the shape of the W dependence of the cross section as a function, $\sigma(W) \sim W^{-12}\beta^*_\Lambda$, where β^*_Λ is the velocity of Λ in the c.m. frame of $\gamma\gamma$. The other is obtained at each $\Delta W = 0.2$ GeV/c^2 bin without this assumption. The latter limit improves the TASSO's limit[11] by about three times in significance. Although the former gives a severer limit than does the latter case, it is still slightly higher than the measured cross section for $p\bar{p}$ production[3]. The expected $\Lambda\bar{\Lambda}$ production cross section is about ten-times smaller than the $p\bar{p}$ production[5]. The present upper limit is too loose to restrict the theoretical models for the $\Lambda\bar{\Lambda}$ production.

We found 3-event candidates of $\gamma\gamma \rightarrow \Lambda\bar{\Lambda} + \gamma$'s. The photon energy is cut at 0.2 GeV. However, we found no candidate for $\Sigma^0 \rightarrow \Lambda\gamma$ decay in these events. Since the energy cut for the photon is higher than the c.m. energy of the decay (74 MeV), the acceptance is too small to detect Σ^0.

8 Conclusion

We studied the baryon-antibaryon inclusive process from two-photon collisions at $<\sqrt{s}>$ = 58 GeV at the KEK e^+e^- collider TRISTAN. The Λ baryons were reconstructed with high purity in the sample. The ratios of the cross sections for $\Lambda\bar{p}$- ($p\bar{\Lambda}$-) and $\Lambda\bar{\Lambda}$-inclusive events over the $p\bar{p}$-inclusive events are consistent with Monte Calro expectations in which the contribution of the s-quark and baryon production from the "sea" is dominant. However, the cross section of the baryon-antibaryon inclusive production showed an excess at low-W_C, at $2 \leq W_C \leq 5$ GeV/c^2, over the MC expectation, where W_C is the invariant mass of the final-state particles emitted to large angles. This fact indicates that there is a defect in baryonization models in the MC at low-W_C region related to higher-order QCD or non-perturbative effects. In the higher W_C region, we found no narrow azimuthal angle correlation between a baryon and an antibaryon, which is expected based on the jet-fragmentation Monte Carlo method. We found no apparent problem in the s-quark or Λ production mechanism, itself, in the Monte Carlo calculations.

We searched for exclusive Λ pair production from two-photon collisions, $\gamma\gamma \rightarrow \Lambda\bar{\Lambda}$. We found no candidate, and the upper limit of the cross section has been obtained.

Acknowledgement
The authors gratefully acknowledge the outstanding efforts of the TRISTAN accelerator group for excellent machine operation. They are indebted to the KEK support groups of cryogenics and computation. Thanks also go to the technical staff of the collaborating institutes, who enabled us to take data continuously.

References

1. H.Terazawa: J. Phys. Soc. Jpn., 47 (1979) 355.
2. M.Drees and R.M.Godbole: Nucl. Phys. B339 (1990) 355; M.Drees and R.M.Godbole: preprint BU-TH-92/5 (1992).
3. M. Artuso et al., CLEO Coll.: Phys. Rev. D50 (1994) 5484.
4. G.Farrar et al.: Nucl. Phys. B259 (1985) 702; B263 (1986) 746(E).
5. M.Anselmino et al.: Intern. J. Mod. Phys. A4 (1989) 5213.
6. P.Kroll et al.: Phys. Lett. B316 (1993) 546.
7. M.Althoff et al., TASSO Coll.: Phys. Lett. B139 (1984) 126; H.Aihara et al., TPC Coll.: Phys. Rev. Lett. 55 (1985) 1047.
8. P.Abreu et al., DELPHI Coll.: Phys. Lett. B318 (1993) 249; P.D.Acton et al., OPAL Coll.: Phys. Lett. B305 (1993) 415.
9. R.Enomoto et al., TOPAZ Coll.: Phys. Lett. B347 (1995) 179.
10. R.Enomoto et al., TOPAZ Coll.: Phys. Lett. B341 (1994) 238.
11. H.Aihara et al., TPC/2γ Coll.: Phys. Rev. D40 (1989) 2772; M.Althoff et al., TASSO Coll.: Phys. Lett. 142B (1984) 135.
12. K.Abe et al., VENUS Coll.: J. Phys. Soc. Jpn., 561 (1987) 3763.
13. R.Arai et al.: Nucl. Instr. and Meth. A217 (1983) 181.
14. Y.Hemmi et al: Jpn. J. Appl. Phys. 26 (1987) 982.
15. T.Sumiyoshi et al.: Nucl. Instrum. Meth. A271 (1988) 432.
16. Y.Fukushima et al.: IEEE Trans. Nucl. Sci. 36 (1989) 670.
17. F.A.Berends, P.H.Daverveldt and R.Kleiss: Nucl. Phys. B253 (1985) 441 and Comp. Phys. Comm. 40 (1986) 285.
18. T.Sjöstrand: preprint CERN-TH.6488/92 (1992).
19. T.Sjöstrand: preprint CERN-TH.7112/93 (1994).
20. Ch. Berger et al., PLUTO Coll.: Phys. Lett. 149B (1984) 421.
21. H.Abramowicz, K.Charchula and A.Levy: Phys. Lett. B269 (1991) 458.
22. S.Uehara et al., VENUS Coll.: Z.Phys. C63 (1994) 213; H.Ohyama: Proceedings of the 2nd Workshop on TRISTAN Physics at High Luminosities, Nov. 24-26, 1993, KEK, Tsukuba, KEK proceedings 93-22 (1994) 359; H.Ohyama: Ph.D. Thesis, J. Sci. Hiroshima University, A59 (1995) 51.
23. R.Enomoto et al. TOPAZ Coll.: Phys. Rev. D50 (1994) 1879; R.Enomoto et al., TOPAZ Coll.: Phys. Lett. B328 (1994) 535; M.Iwasaki et al., TOPAZ Coll.: Phys. Lett. B341 (1994) 99.
24. M.Drees and K.Grassie: Z. Phys. C28 (1985) 451.
25. R.Tanaka et al., AMY Coll.: Phys. Lett. B277 (1992) 215; R.Tanaka: KEK preprint 92-37 (1992); D.Buskulic et al., ALEPH Coll.: Phys. Lett. B313 (1993) 509; H.Hayashii et al., TOPAZ Coll.: Phys. Lett. B314 (1993) 149.

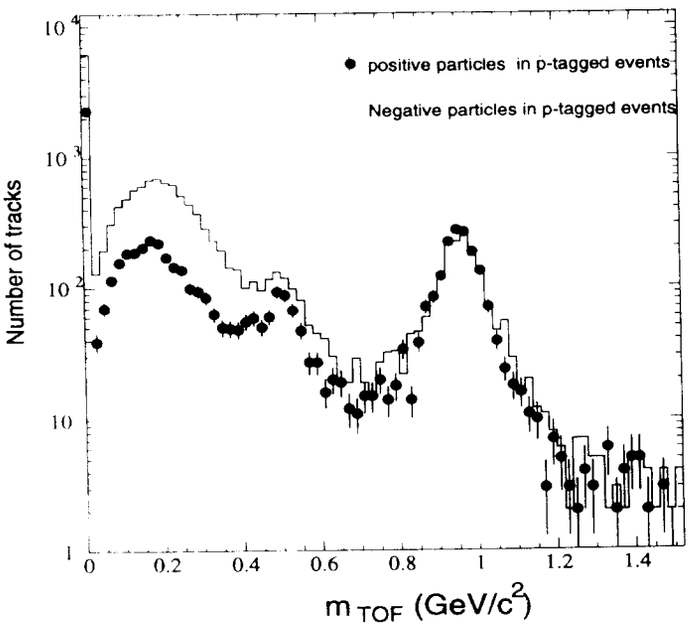

Figure 1: Mass distributions for charged particles measured by the TOF. The dots with error bars (histogram) are for positive (negative) particles for events which contain an antiproton (a proton) candidates. The leftmost bin includes entries from tracks whose measured $m^2_{\rm TOF}$ is less than 0 or having no associating TOF hits.

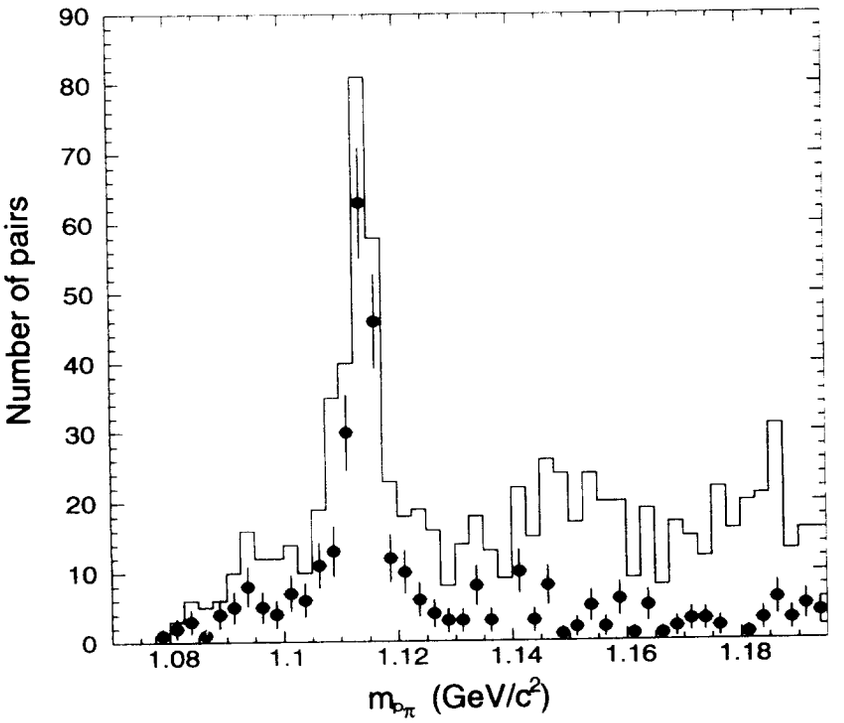

Figure 2: Invariant mass distributions ($m_{p\pi}$) around the Λ mass region. The histogram is before applying the decay length cut and the dots with error bars after the cut.

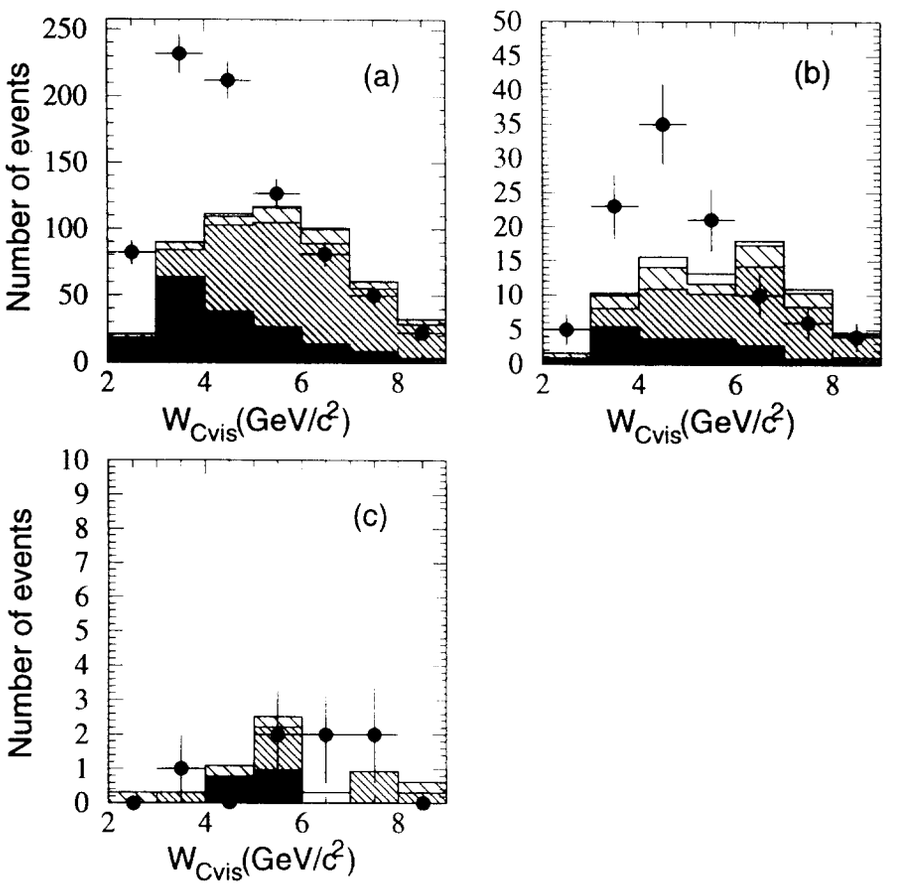

Figure 3: Distributions for visible invariant mass for final-state particles at large angles, W_{Cvis}, for (a)$p\bar{p}X$, (b)$\Lambda\bar{p}X$ or $p\bar{\Lambda}X$ and (c) $\Lambda\bar{\Lambda}X$ events. The histograms are the expectations from the MC: Dark region for 1) (direct processes other than primary $s\bar{s}$ production), darkly hatched for 2)(resolved photon processes other than primary $s\bar{s}$ production), lightly hatched for 3)(primary $s\bar{s}$ production) and opened for 4)(Λ_c decay) for the four classes of the MC described in subsection 6.2.

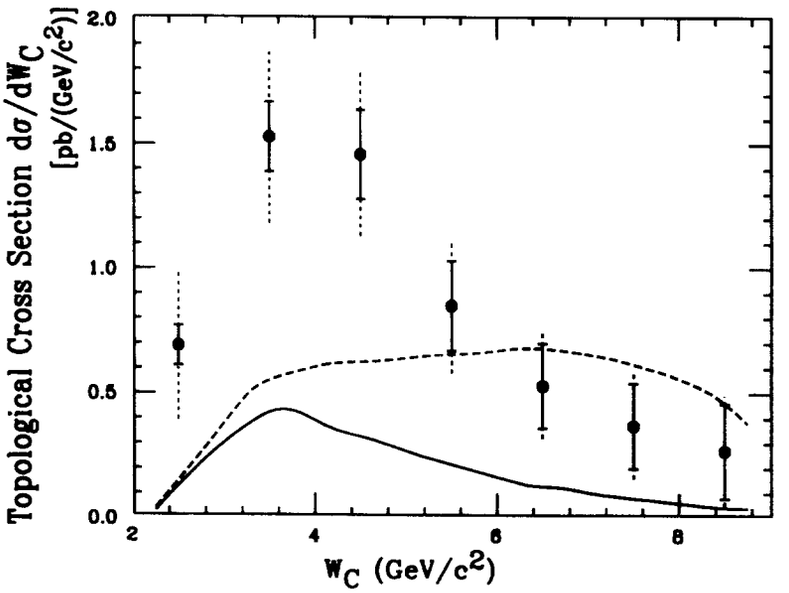

Figure 4: Topological cross section for $p\bar{p}$-inclusive events in no-tagged two-photon processes. The definition is Eqs. (1) and (2) in subsection 6.3. The error bars with solid and dashed lines show the statistical and systematic errors, respectively. The solid curve is a prediction of the direct processes, and the dashed curve the sum of the direct and resolved photon processes.

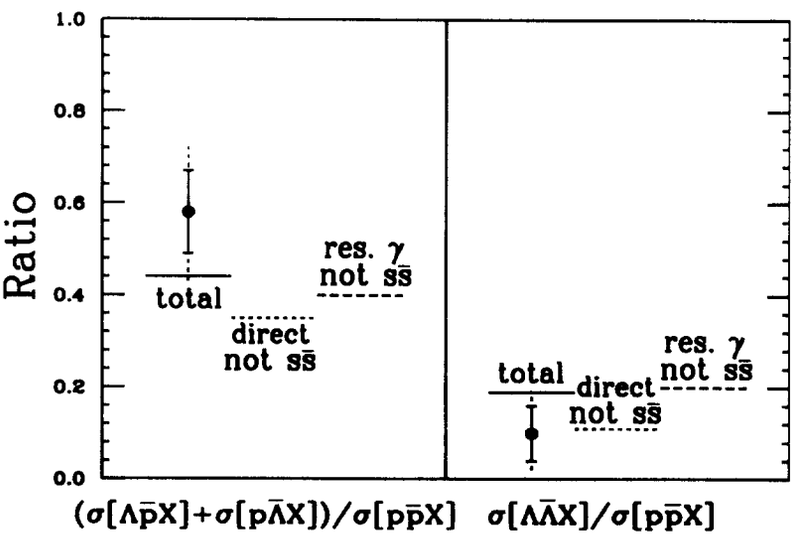

Figure 5: Baryon-antibaryon flavor ratios, $(\sigma[p\bar{\Lambda}X] + \sigma[\Lambda\bar{p}X])/\sigma[p\bar{p}X]$ and $\sigma[\Lambda\bar{\Lambda}X]/\sigma[p\bar{p}X]$. The experimental results (dots with error bars) are compared with the MC expectations for total contributions, for 1) (direct processes other than primary $s\bar{s}$ production) and for 2)(resolved photon processes other than primary $s\bar{s}$ production) of the categories described in subsection 6.2. The error bars with solid and dashed lines show the statistical and systematic errors, respectively.

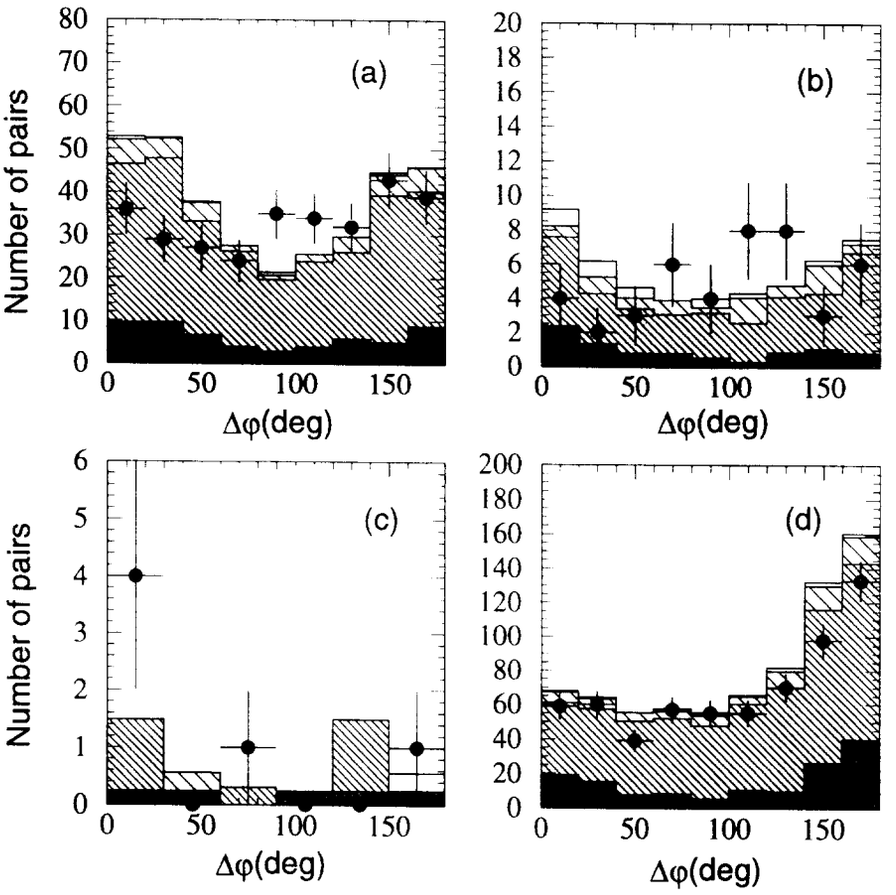

Figure 6: Distributions for the azimuthal angle difference ($\Delta\varphi$) between a baryon and an antibaryon in (a) $p\bar{p}X$ (b)$\Lambda\bar{p}X$ or $p\bar{\Lambda}X$ and (c) $\Lambda\bar{\Lambda}X$ events, and (d) between a baryon (an antibaryon) and other charged particles than an antibaryon (a baryon) for the baryon-antibaryon inclusive events at $W_{\mathrm{Cvis}} \geq 5\mathrm{GeV}/c^2$. The histograms are the MC expectations (see the caption for Fig.3).

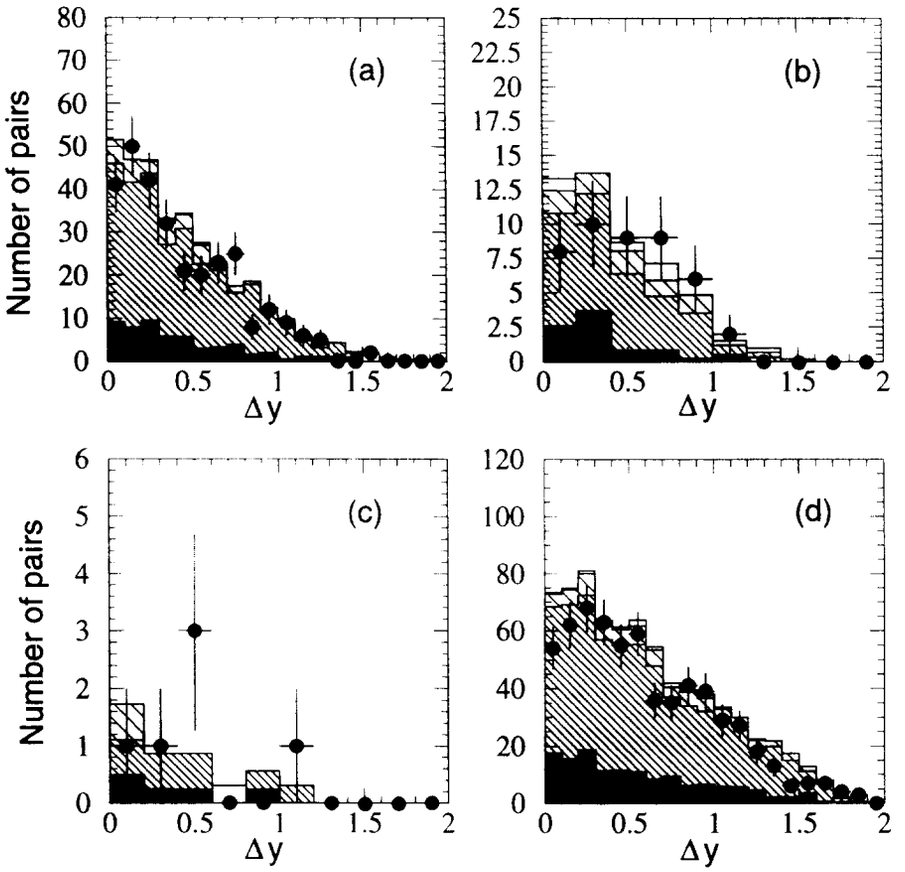

Figure 7: Distributions for the rapidity difference (Δy) between a baryon and an antibaryon in (a) $p\bar{p}X$ (b)$\Lambda\bar{p}X$ or $p\bar{\Lambda}X$ and (c) $\Lambda\bar{\Lambda}X$ events, and (d) between a baryon (an antibaryon) and other charged particles than an antibaryon (a baryon) for the baryon-antibaryon inclusive events at $W_{\mathrm{Cvis}} \geq 5\mathrm{GeV}/c^2$. The histograms are the MC expectations (see the caption for Fig.3).

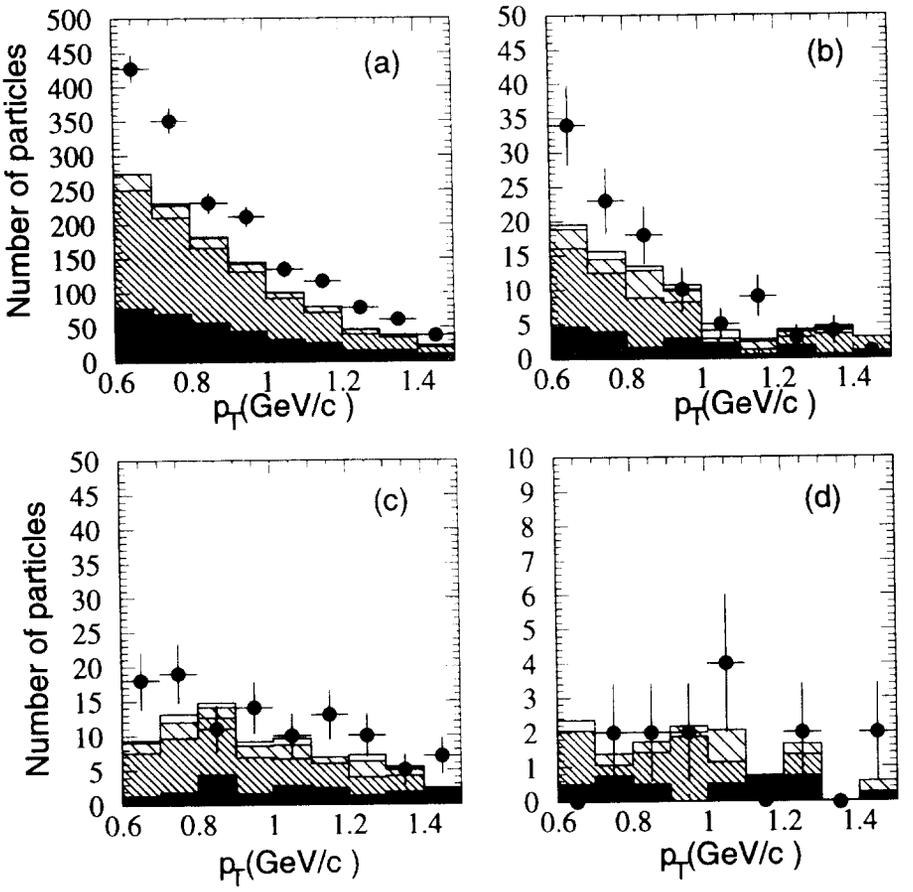

Figure 8: Transverse momentum distributions for baryons and antibaryons, (a) for p ($\bar{p}$) in $p\bar{p}X$ events, (b) for p ($\bar{p}$) in $\Lambda\bar{p}X$ or $p\bar{\Lambda}X$ events, (c) for Λ ($\bar{\Lambda}$) in $\Lambda\bar{p}X$ or $p\bar{\Lambda}X$ events and (d) for Λ ($\bar{\Lambda}$) in $\Lambda\bar{\Lambda}X$ events. The histograms are the MC expectations (see the caption for Fig.3). No W_{Cvis} cut was applied.

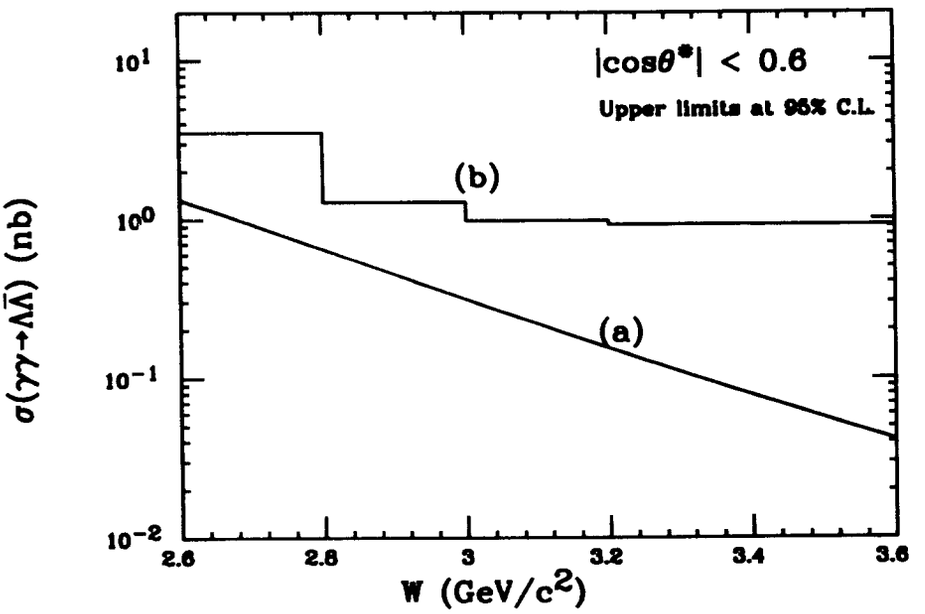

Figure 9: Upper limits at the 95% confidence level for the cross section for $\gamma\gamma \to \Lambda\bar{\Lambda}$ process for the polar angle range in the two-photon c.m.system $|\cos\theta^*| \leq 0.6$ (a) with assuming the shape of the W-dependence as $\sim W^{-12}\beta_\Lambda^*$ and (b) without such an assumption.